THE ASTROPHYSICAL JOURNAL, 419:585–595, 1993 December 20

DETECTION OF H92α RECOMBINATION LINE FROM THE GALAXIES NGC 3628, IC 694, AND NGC 1365

K. R. ANANTHARAMAIAH
Raman Research Institute, Bangalore 560 080, India
JUN-HUI ZHAO AND W. M. GOSS
National Radio Astronomy Observatory, Very Large Array, P.O. Box O, Socorro NM 87801
AND
F. VIALLEFOND
DEMIRM, Observatoire de Meudon, F-92190 Meudon, France
Received 1993 April 12; accepted 1993 June 29

ABSTRACT

Using the Very Large Array with an angular resolution of $\sim 3''$, we have detected the hydrogen recombination line H92α (v_{rest} = 8309.38 MHz) from the starburst nuclei in the galaxies NGC 3628 and IC 694 and also from the Seyfert II nucleus in NGC 1365. In each case the line-emitting region extends over a few hundred parsecs. The detected lines have peak intensities in the range 0.5–1.5 mJy and widths (FWHM) 200–400 km s^{-1}. The line was not detected in three other galaxies (NGC 262, NGC 1068, and NGC 3079) that were observed to a similar sensitivity level.

We present a model in which a collection of H II regions in the nuclear region accounts for the observed H92α line. The required number of H II regions, their temperature, electron density, and linear size are constrained by the observed line flux density, line width, continuum spectrum, and size of the line-emitting region. If the temperature of the H II regions is above 5000 K, then electron densities in the range 5–50 × 10^3 cm^{-3} are permitted by the available constraints. Several hundred H II regions of a few parsecs in size, with a total mass of a few times 10^5 $M_\odot$, are required to account for the observed line flux density. The rate of production of Lyman continuum photons required to maintain the ionization is a few times 10^{54} s^{-1}. Much of the line emission comes from internal stimulated emission due to the continuum generated within the H II regions which account for 5%–30% of the observed total continuum at 5 GHz. Predictions are made for the expected recombination line and continuum flux density as a function of frequency from the nuclear region of the galaxies.

Subject headings: galaxies: individual (NGC 1365, NGC 3628, IC 694) — galaxies: nuclei — radio lines: galaxies

1. INTRODUCTION

In contrast to their usefulness in studying a variety of ionized regions in the Galaxy, radio recombination lines (RRLs) have had very little impact on the study of external galaxies. Although calculations by Shaver (1978) showed that the prospects for detecting RRLs from galaxies and quasars are quite good, RRLs have been detected in only three external galaxies beyond the Magellanic Clouds, namely M82 (Shaver, Churchwell, & Rots 1977), NGC 253 (Seaquist & Bell 1977), and NGC 2146 (Puxley et al. 1991). Several searches made toward a number of galaxies and quasars have yielded no new detections (Churchwell & Shaver 1979; Bell & Seaquist 1978; Bell et al. 1984). As discussed by Shaver (1978) and Sarazin & Wadiak (1983), detection of RRLs from distant extragalactic sources could be useful in several respects; e.g., the study of physical conditions and velocity fields in the nuclei of galaxies and the determination of distances to quasars by comparing the fluxes of radio and optical recombination lines.

In this paper we present the first results of a new search program for RRLs in extragalactic sources using the Very Large Array (VLA). We were motivated to undertake this renewed attempt by the results of interferometric observations of RRLs at wavelengths of 20, 6, and 3.6 cms toward the nearby starburst galaxy NGC 253 (Anantharamaiah & Goss 1989). These observations indicated that the RRLs arise only in the nuclear region of the galaxy and that the most favorable wavelength for searching RRLs in similar galaxies, using the VLA, is near 3.6 cm (e.g., H92α line). The expected line strengths are ~1 mJy, which the present VLA receiver system can detect using integration times of a few hours. In contrast, the previous searches had set upper limits to the line strengths of 5–10 mJy (Bell & Seaquist 1978; Bell et al. 1984).

In this initial search, we observed six galaxies which can be divided into two categories: (1) spiral galaxies with a bright radio continuum core (NGC 3079, NGC 3628, and IC 694/NGC 3690) and evidence for "starburst" activity near the nucleus and (2) Seyfert type II galaxies (NGC 262, NGC 1068, and NGC 1365) with a bright radio continuum core. Seyfert II galaxies have a narrow line region (line width ~500 km s^{-1}), with physical conditions which are not unlike galactic H II regions or starburst nuclei although the ionization is believed to be due to the central source with a power-law spectrum (Osterbrock 1989). RRLs could be expected from these sources because of stimulated emission. This search has yielded detection in two of the three starburst galaxies that were observed (NGC 3628 and IC 694) and also from the Seyfert II galaxy NGC 1365. This paper is organized as follows. In the next two sections details of the observations and the results are presented. In § 4, we assess the nature of the ionized gas by considering a uniform slab model and a model with a collec-

TABLE 1

LOG OF RRL (H92α) OBSERVATIONS WITH THE VLA

Galaxy (1)	Type (2)	α(1950) (3)	δ(1950) (4)	V_{Hel} (km s^{-1}) (5)	φ-Cal (6)	BP-Cal (7)
NGC 0262	Seyfert II	00^{h}46^{m}04^s.0	+31°41′04″	4530	3C 48	3C 48
NGC 1068	Seyfert II	02 40 06.5	−00 13 32	1120	0237−027	3C 84
NGC 1365	Seyfert II	03 31 42.0	−36 18 30	1650	0402−362	0402−362
NGC 3079	Sbc	09 58 35.0	+55 55 15	1150	1031+567	3C 84
NGC 3628	S3pec	11 17 40.0	+13 51 46	845	1119+183	3C 286
IC 694/NGC 3690	Sc+Sc	11 25 44.2	+58 50 23	3100	1144+542	3C 286

tion of H II regions in the nuclear region of these galaxies. The implications of the results are discussed in § 5. Throughout this paper, we use $H_0 = 75$ km s^{-1} Mpc^{-1}.

2. OBSERVATIONS AND DATA PROCESSING

Observations were made during 1990 October when the VLA was in the C-configuration, which gives an angular resolution of ∼2″.5 at 8.4 GHz. We use 15 spectral channels covering a bandwidth of 25 MHz which corresponds to a velocity coverage of about 850 km s^{-1} for the H92α line (ν_{rest} = 8309.3832 MHz). After Hanning smoothing (which was applied on-line) the frequency resolution is 1.56 MHz (56.4 km s^{-1}). Each source was observed for about 6 hr. Table 1 gives the list of observed sources, their positions, the heliocentric velocity (col. [5]), calibrator used for correcting instrumental phase (col. [6]), and the calibrator used for correcting the frequency response (bandpass) of the system (col. [7]). The amplitude scale was set by observing the sources 3C 48 ($S_{3.6\ cm}$ = 3.36 Jy) and 3C 286 ($S_{3.6\ cm}$ = 5.33 Jy).

Further processing of the data was carried out using the Astronomical Image Processing System (AIPS) developed by NRAO. Phase corrections obtained from self-calibration of the continuum channel (which is the average of the central three-quarters of the observed 25 MHz band) was applied to all the line channel data. Continuum emission from the line data was subtracted using the method UVLIN (Cornwell, Uson, & Haddad 1992), in which the continuum is determined for each baseline by a linear fit to the outer channels where no line was expected. The final continuum and line images were made using natural weighting of the visibility data to achieve maximum possible signal-to-noise ratio. Typically, the rms noise in the channel images is ∼100 μJy beam^{-1}.

3. OBSERVATIONAL RESULTS

3.1. *Detections*

H92α line emission was detected in the starburst galaxies NGC 3628 and IC 694 (sometimes referred to in the literature as NGC 3690 A) and also in the Seyfert II galaxy NGC 1365. In all three galaxies the line emission is observed only in the nuclear region, generally coincident with the brightest continuum emission. The observed line and continuum parameters are presented in Table 2. The line emission is spatially resolved in NGC 3628 and NGC 1365. In Figures 1 and 2, we present the continuum images of the three galaxies and the H92α profiles integrated over the line region, respectively. The centroid velocities of the H92α line generally agree with the observed H I or CO velocities at a level of 50 km s^{-1}.

3.1.1. *NGC 3628*

NGC 3628 is an edge-on (i = 89°) Sbc galaxy and is a part of an interacting complex of spiral galaxies called the Leo Triplet Arp 217. The inferred distance is 11 Mpc. NGC 3628 has a prominent radio continuum core similar to the prototype starburst galaxy NGC 253 (see Fig. 1*a*). The radio continuum is

TABLE 2

OBSERVED LINE AND CONTINUUM PARAMETERS OF DETECTED SOURCES

Parameter (1)	NGC 3628 (2)	IC 694 (3)	NGC 1365 (4)
Peak line flux density (mJy)[a]	1.4 ± 0.09	0.47 ± 0.10	0.99 ± 0.10
Velocity dispersion (km s^{-1})	99 ± 26	149 ± 40	144 ± 30
Integrated line flux (10^{-23} W m^{-2})	8.6 ± 1.5	3.9 ± 1.0	12 ± 2
Continuum flux density over line region (mJy)[b]	64.4 ± 0.1	88.8 ± 0.1	48.3 ± 0.2
Centroid heliocentric velocity (km s^{-1})	864 ± 56	3020 ± 90	1670 ± 80
Beam size (" × ", PA)	3.5 × 3.2, −57°	3.0 × 2.9, −19°	8.0 × 3.1, 0°
No. of beam areas where line is observed	8.6	2.6	8.4
Line width (FWHM in km s^{-1})	170 ± 70	350 ± 110	310 ± 110
Distance (Mpc)	11.5	40.3	22.0
Continuum flux density at 1.4 GHz (mJy)	191 ± 10[c]	190 ± 20[c]	108[d]
Continuum flux density at 4.9 GHz (mJy)	66 ± 10[c]	110 ± 15[c]	53[d]
Continuum flux density at 15 GHz (mJy)	>23[e]	>61[e]	
Estimated thermal continuum flux density at 5 GHz (mJy)	21[f]	18[f]	22

[a] After integrating over the line region.
[b] Integrated continuum flux density over the region where the line detected.
[c] Taken from Condon et al. 1982.
[d] Taken from Sandqvist et al. 1982.
[e] Taken from Carral et al. 1990.
[f] Taken from Ho et al. 1990.

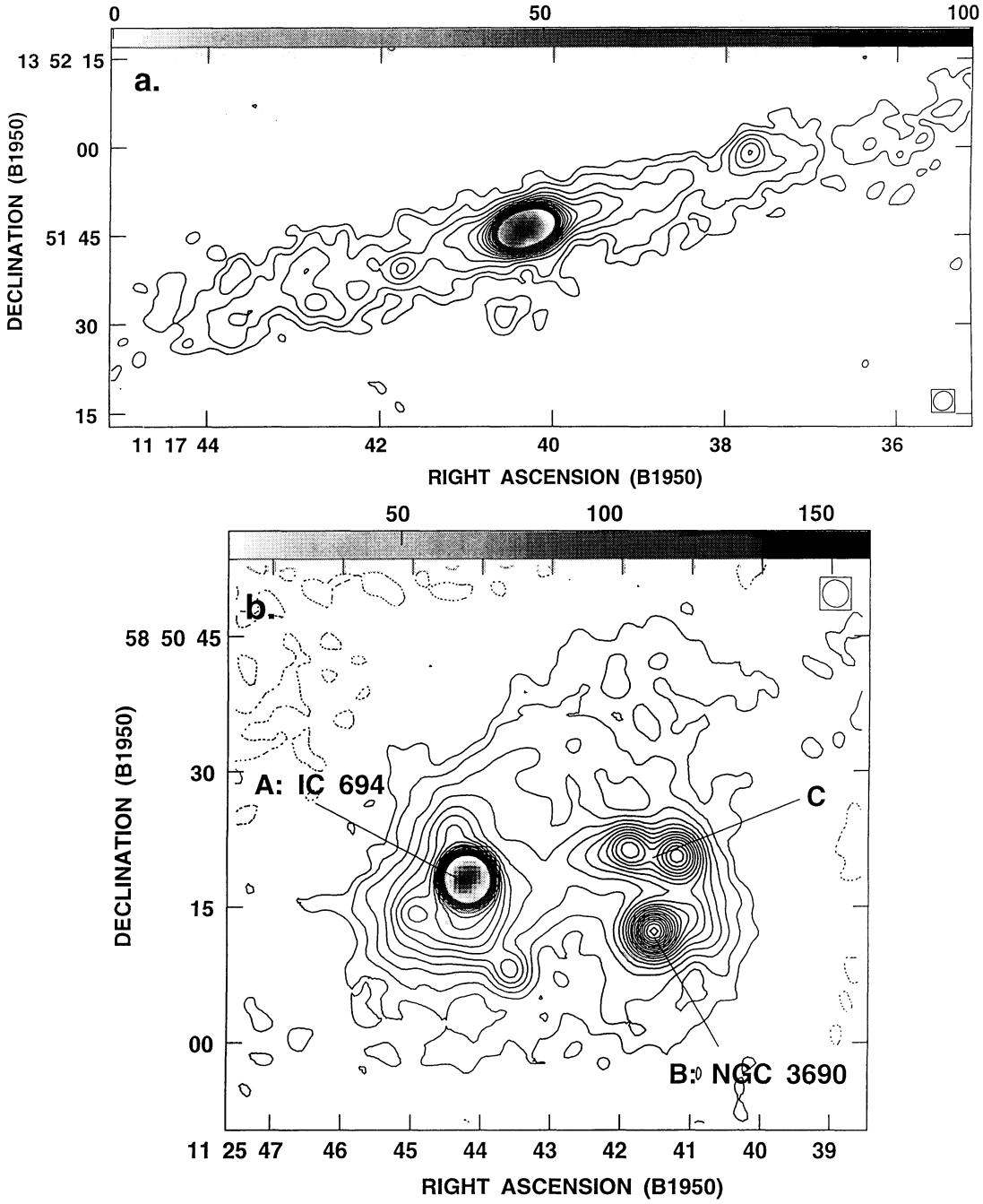

FIG. 1.—(*a*) Continuum image of NGC 3628 obtained from the H92α observations using the VLA with the beam size (FWHM) of 3″.5 × 3″.2 (−57°) indicated in the lower right corner. The contour levels are −0.1, 0.05, 0.1, 0.2, 0.35, 0.55, 0.8, 1.1, 1.5, 1.9... mJy beam^{-1}. The H92α line detected in the nuclear region is indicated by a linear gray-scale representation of line intensity (0–100 mJy beam^{-1} km s^{-1}). (*b*) Continuum image of IC 694/NGC 3690 obtained from the H92 α observations using the VLA with a beam size (FWHM) of 3″.0 × 2″.9 (−19°) indicated in the upper right corner. The contour levels are −0.1, 0.1, 0.2, 0.4, 0.7, 1.1, 1.6, 2.6, 2.9, 3.7, 4.5, 5.6, 6.7, 7.9, 9.2, 10.6, 12.1, 13.7, 15.4 mJy beam^{-1}. The H92α line detected in the nuclear region of IC 694 is indicated by a linear gray-scale representation of line intensity (10–160 mJy beam^{-1} km s^{-1}). No H92α line emission has been detected from the nucleus of NGC 3690. (*c*) Continuum image of NGC 1365 obtained from the H92α observations using the VLA with a beam size (FWHM) of 8″.0 × 3″.1 (0°) indicated in the upper right corner. The contour levels are −0.1, 0.1, 0.2, 0.4, 0.7, 1.1, 1.6, 2.6, 2.9, 3.7, 4.5, 5.6, 6.7, 7.9, 9.2, 10.6 mJy beam^{-1}. The H92α line detected in the nuclear region is indicated by a linear gray-scale representation of line intensity (0–60 mJy beam^{-1} km s^{-1}).

predominantly nonthermal with a spectral index $\alpha = -0.86$ (where $S \propto \nu^{\alpha}$) between 20 and 6 cm (Condon et al. 1982). High-resolution observations at 2 cm (Carral, Turner, & Ho 1990) reveal that the central bright source is made up of at least a dozen smaller sources with size scales of a few parsecs. Complex kinematics near the nuclear region have been revealed by observations of H I, OH, and H_2CO absorption lines (Schmelz, Baan, & Haschik 1987a, b; Baan & Goss 1992). X-ray and Hα observations (Fabiano, Heckman, & Keel 1990) have provided evidence for a collimated outflow from the nuclear region. Molecular gas, as revealed by CO observations (Israel, Baas, & Maloney 1990; Boisse, Casoli, & Combes

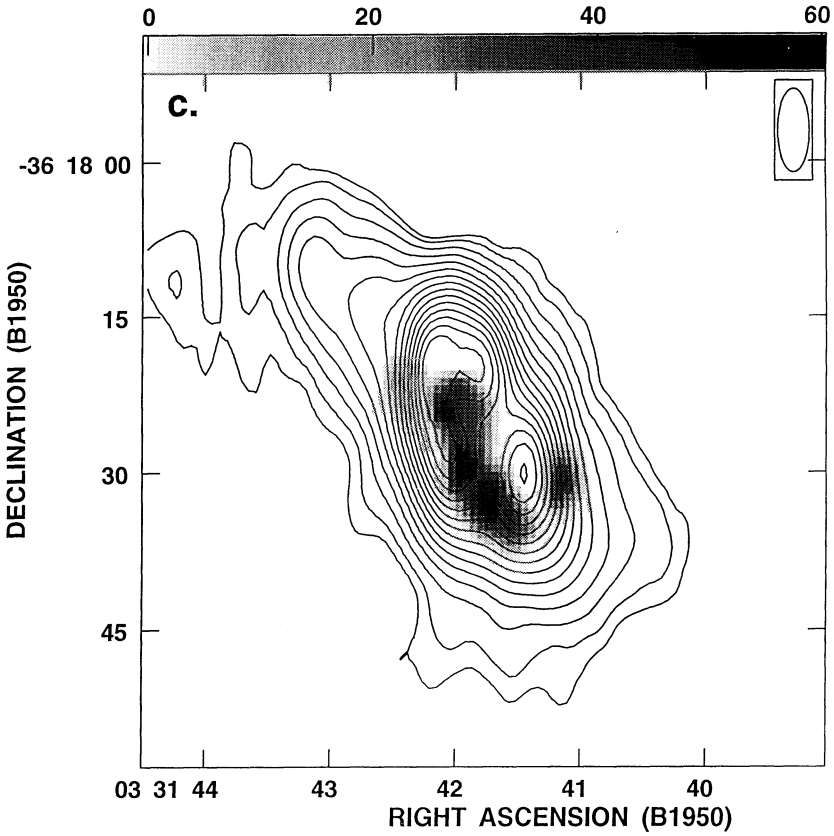

FIG. 1—*Continued*

1987), is strongly peaked near the center. Figure 2*a* shows the H92α spectrum integrated over the line emission region.

In Figure 3*a* we present the spatial distribution of the velocity-integrated H92α line. The peak of the line emission is coincident with the continuum peak and extends over about 10″ in the nuclear region. The observed velocity field of the ionized gas is presented in Figure 3*b*, and a position-velocity diagram along the major axis of the galaxy is shown in Figure 3*c*. A rotating nuclear disk of about 5″ in diameter centered around 900 km s^{-1} is obvious in this diagram. Some diffuse ionized gas extending about 10″ to the east is also obvious in Figure 3*c*. Furthermore, an anomalous feature near 750 km s^{-1} is present at a few arcseconds west of the nucleus. The rotating disk and the anomalous feature are also seen in the higher angular resolution H_2CO (Baan & Goss 1992), OH, and H I (Schmelz et al. 1987a, b) observations. It has been suggested (Rots 1978; Baan & Goss 1992) that the perturbed velocity field in the nuclear region of NGC 3628 is a result of an encounter with the companion galaxy NGC 3627.

3.1.2. *IC 694/NGC 3690*

IC 694 and NGC 3690 are an interacting pair of galaxies, also known as Arp 299, at a distance of 41 Mpc. In the radio continuum image shown in Figure 1*b*, the source labeled A is IC 694, B is NGC 3690, and C is the interface region of the two galaxies. In the literature the entire system is sometimes referred to as NGC 3690 with labels A, B, C, etc., for the different components. In the present observations, the H92α line has been detected only in IC 694. Detailed optical, infrared, and radio observations of this interacting pair have been performed by Gehrz, Sramek, & Weedman (1983), who argue that several episodes of starburst have occurred in different locations of this system. This interacting system has been recognized as an ultraluminous IR source (Young et al. 1989). Interferometric CO observations (Sargent & Scoville 1991) have revealed a major gas condensation at the nuclei of both galaxies IC 694 and NGC 3690 and in the interface region. A large mass of gas ($4 \times 10^9\ M_\odot$) within the central 250 pc of IC 694, inferred from CO observations (Sargent & Scoville 1991), suggested either a very concentrated starburst or the presence of a central Active Galactic Nucleus (AGN). Earlier radio observations by Gehrz et al. (1983) found a compact component in IC 694 with a relatively flat spectral index of $\alpha = -0.34$ between 1.49 and 4.9 GHz; the authors had argued that the source is synchrotron self-absorbed and hence to compact to be due to starburst. Recent high-resolution continuum observations at 8.4 GHz (Condon et al. 1991) have resolved the compact radio source. The brightness temperature of the central source is $\sim 10^4$ K at 8.4 GHz.

The H92α line detected in IC 694 is marginally spatially resolved with a beam of $\sim$3.″0, which implies a linear size of about 600 pc. The detection of RRL from the nuclei of IC 694 and the relatively low continuum brightness temperature observed by Condon et al. (1991) favors the starburst hypothesis. This object is the most distant galaxy (41 Mpc) from which a radio recombination line is detected in the present observations.

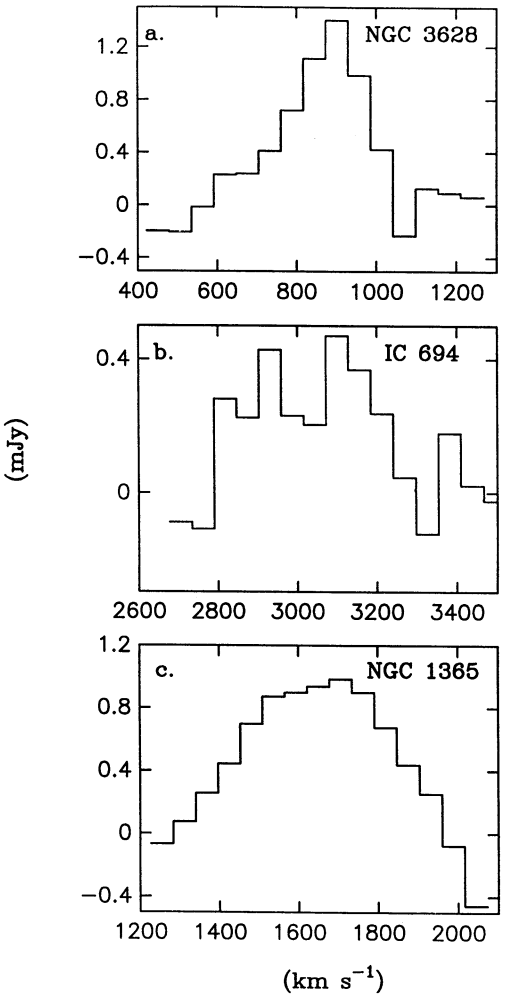

FIG. 2.—Integrated H92α line profile of NGC 3628 (*a*), IC 694 (*b*), and NGC 1365 (*c*). The horizontal axis indicates the heliocentric velocity.

3.1.3. *NGC 1365*

NGC 1365 is a barred, two-armed grand design spiral galaxy of type SBb at an inferred distance of 22 Mpc. The nuclear spectrum has Seyfert type II characteristics with evidence for the presence of normal H II regions (Edmunds & Pagel 1982). The complex velocity field in the nuclear region has been studied in Hα by Teuben et al. (1986). Very little H I gas is observed in the central region (Ondrechen & van der Hulst 1989). Radio continuum observations (Sandqvist, Jorsater, & Lindblad 1982) show several nonthermal components in the nuclear regions with a mean spectral index $\alpha = -0.72$ between 1.4 and 4.9 GHz. The radio continuum image at 8.3 GHz and the integrated H92α profile in the nuclear region are shown in Figures 1*c* and 2*c*, respectively.

The present observations have detected the H92α line in the nuclear region with a line width (FWHM) of ~400 km s^{-1}. The line emission is spatially resolved and its position is slightly offset from the continuum peaks. The spatial distribution of the integrated line emission and the observed velocity field are presented in Figures 4*a* and 4*b*. This is the first Seyfert-type galaxy from which a RRL has been detected. The line arises likely in a narrow-line region which is typical of a Seyfert II galaxy.

3.2. *Nondetections*

The H92α line was not detected in the three other galaxies observed (NGC 262, NGC 1068, and NGC 3079). Puxley et al. (1991) have reported a marginal detection ($< 3\ \sigma$) of the H35α line from NGC 1068. We have also not detected any line emission in NGC 3690 which is interacting with IC 694 discussed above. The continuum images of the three galaxies where no line is detected are presented in Figure 5. The continuum flux density in the nuclear region and the upper limits to the line strength are presented in Table 3. It should be noted that these observations cannot detect lines with FWHM in excess of ~450–500 km s^{-1}, as the total velocity coverage is ~850 km s^{-1}. The Seyfert II nuclei in the galaxies NGC 262 and NGC 1068 do show Hα line widths of 422 ± 30 and 734 ± 40 km s^{-1}, respectively (Wilson & Nath 1990). If the radio lines are of comparable width, then it may still be possible to detect RRLs from these two galaxies using a wider velocity coverage.

4. THE NATURE OF THE IONIZED GAS

The ionized gas that produces the observed H92α line must satisfy an important constraint. In all three galaxies (NGC 3628, NGC 1365, and IC 694) detected with the H92α line, the radio continuum in the nuclear region has a nonthermal spectrum. The dominant nonthermal flux density in the nuclei implies that the thermal emission from the ionized region must only be a small fraction of the observed continuum flux density. For instance, the measured flux density in the central 10″ region of NGC 3628 is 66 mJy at 4.9 GHz with a spectral index of −0.86 between 1.4 and 4.9 GHz (Condon et al. 1982). If we assume that the observed continuum is the sum of nonthermal emission with a spectral index $\alpha = -1.0$ and optically thin thermal emission ($\alpha = -0.1$), then the thermal contribution at 4.9 GHz is ~15 mJy. In order to determine the nature of the ionized gas in the central region that can satisfy this constraint, we consider two simple models: (1) a uniform slab

TABLE 3

NONDETECTIONS AND UPPER LIMITS

Galaxy (1)	S_c (mJy beam^{-1}) (2)	$S_L(3\ \sigma)$ (mJy beam^{-1}) (3)	S_L/S_C[a] 10^{-2} (4)	Beam (FWHM) (5)
NGC 0262	311	<0.3	<0.1	2″.9 × 2″.9 (54°)
NGC 1068	363	<0.3	<0.1	3″.5 × 2″.9 (4°)
NGC 3079	101	<0.3	<0.3	3″.0 × 2″.9 (20°)
NGC 3690[b]	16	<0.3	<2	3″.0 × 2″.9 (−19°)

[a] The line-to-continuum ratio corresponds only to the region where the continuum peak locates.
[b] The nucleus of NGC 3690 is 22″ southwest to the nucleus of IC 694 where the line has been detected.

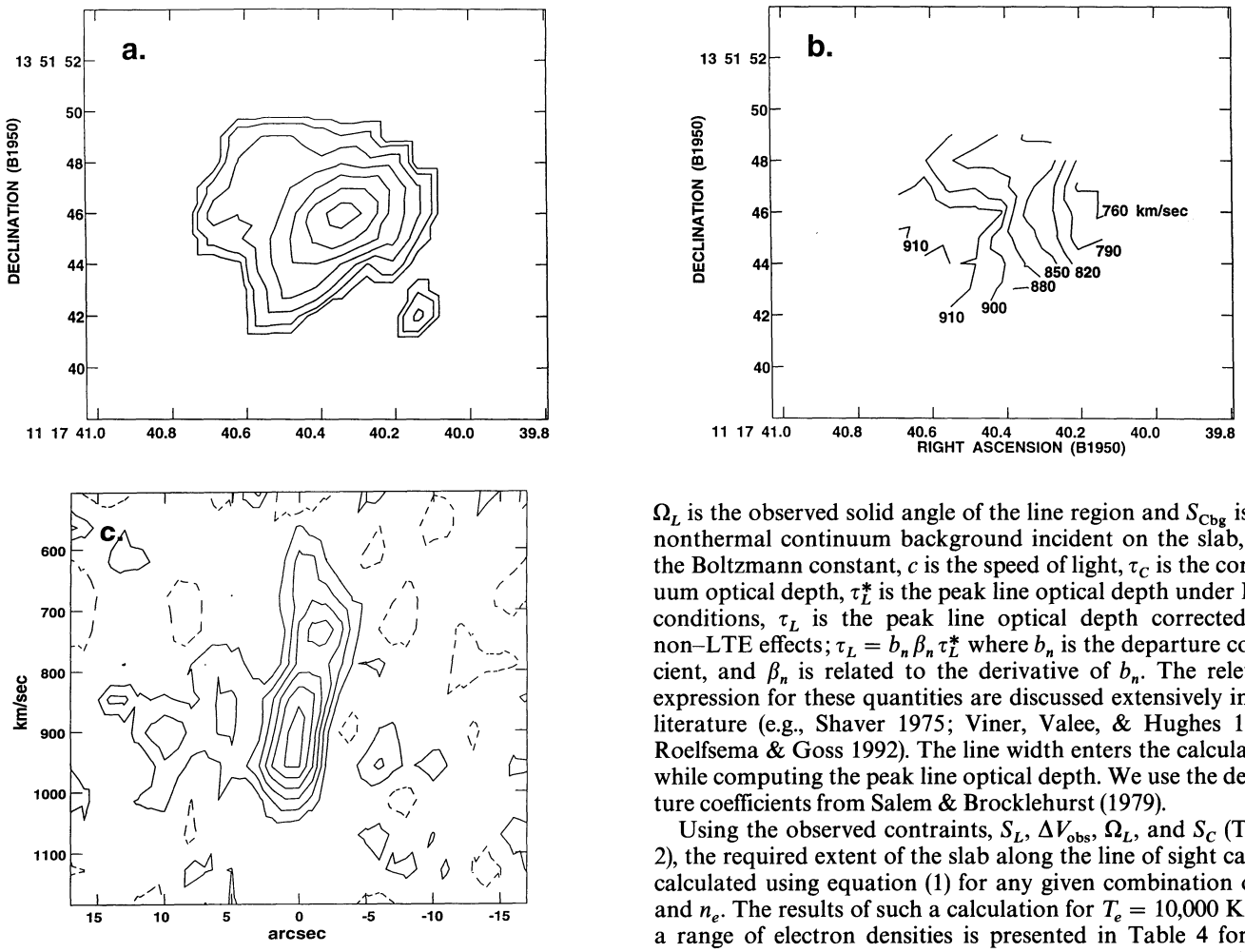

FIG. 3.—(*a*) Spatial distribution of the integrated H92α line emission of NGC 3628. Contour levels are 5, 10, 20, 35, 55, 80, 110 mJy beam^{-1} km s^{-1}; the beam size (FWHM) is 3".5 × 3".2 (−57°). (*b*) Velocity field of NGC 3628 obtained from the H92α line observations. The solid contours represent heliocentric velocity indicated with numbers in units of km s^{-1}. (*c*) Position velocity diagram of NGC 3628 made along the major axis of the galaxy with a position angle −75°. The contours are −0.08, 0.08, 0.16, 0.24, 0.32, 0.40, 0.48 mJy beam^{-1}. The beam size (FWHM) is 3".5 × 3".2 (−57°). The reference position corresponds to R.A.(1950) = 11^{h}17^{m}40^s.34, Decl.(1950) = 13°51'46".0.

of ionized gas in front of the nonthermal source and (2) a collection of H II regions within the central few hundred parsecs.

4.1. *Uniform Slab of Ionized Gas*

If the electron density n_e, electron temperature T_e, and extent of the slab along the line of sight l is specified, then the peak recombination line flux density at a frequency ν can be calculated using

$$S_L = \frac{2k\nu^2}{c^2}\,\Omega_L\,T_e\left[\frac{b_m\tau_L^* + \tau_c}{\tau_L + \tau_c}\,(1 - e^{-\overline{\tau_L + \tau_c}}) - (1 - e^{-\tau_c})\right] + S_{\rm Cbg}\,e^{-\tau_c}(e^{-\tau_L} - 1)\,. \quad (1)$$

The first term in the above equation represents the internal line emission of the slab including stimulated emission due to its own continuum while the second term represents stimulated emission due to the background continuum. In equation (1), Ω_L is the observed solid angle of the line region and $S_{\rm Cbg}$ is the nonthermal continuum background incident on the slab, k is the Boltzmann constant, c is the speed of light, τ_C is the continuum optical depth, τ_L^* is the peak line optical depth under LTE conditions, τ_L is the peak line optical depth corrected for non–LTE effects; $\tau_L = b_n\beta_n\tau_L^*$ where b_n is the departure coefficient, and β_n is related to the derivative of b_n. The relevant expression for these quantities are discussed extensively in the literature (e.g., Shaver 1975; Viner, Valee, & Hughes 1979; Roelfsema & Goss 1992). The line width enters the calculation while computing the peak line optical depth. We use the departure coefficients from Salem & Brocklehurst (1979).

Using the observed contraints, S_L, $\Delta V_{\rm obs}$, Ω_L, and S_C (Table 2), the required extent of the slab along the line of sight can be calculated using equation (1) for any given combination of T_e and n_e. The results of such a calculation for T_e = 10,000 K and a range of electron densities is presented in Table 4 for the source NGC 3628. Column (1) is the electron density, column (2) is the required line of sight extent of the slab, column (3) is the contribution to the line strength from the first term of equation (1), column (4) is the contribution due to the second term, and column (5) is the total thermal continuum emission from the slab at 5 GHz. As the observed total continuum flux density from the nuclear region is 66 mJy at 5 GHz, it is clear from column (5) of Table 4 that a simple uniform slab at T_e = 10^4 K cannot fit the observations for any density. A fit can be obtained in this model only if the temperature is less than about 2500 K. It is also clear from columns (3) and (4) of Table 4 that stimulated emission due to the nonthermal background makes little contribution to the line strength even at low den-

TABLE 4

PARAMETERS OF UNIFORM SLAB MODEL AT T_e = 10,000 K FOR NGC 3628

n_e (cm^{-3}) (1)	Pathlength l (pc) (2)	S_L (1st term) (mJy) (3)	S_L (2nd term) (mJy) (4)	$S_{\rm th}^{5\ {\rm GHz}}$ (mJy) (5)
10	9600	1.3	0.10	150
50	320	1.2	0.19	120
100	77	1.2	0.19	120
500	3.1	1.3	0.14	120
10^3	0.8	1.3	0.11	120
5×10^3 ...	0.03	1.4	0.05	130
10^4	0.009	1.4	0.03	140
10^5	10^{-4}	1.4	0.01	160

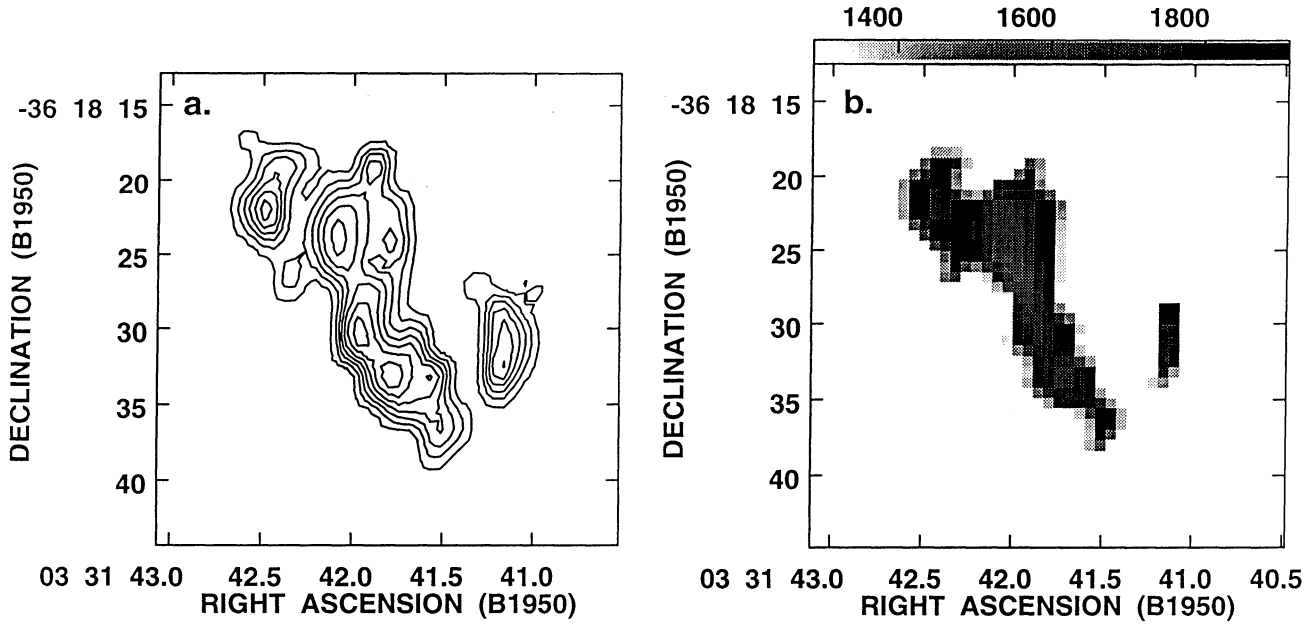

FIG. 4.—(*a*) Spatial distribution of the integrated H92α line emission of NGC 1365. Contour levels are 5, 15, 25, 35, 45, 55, 65 mJy beam^{-1} km s^{-1}; the beam size (FWHM) is 8.″0 × 3.″1 (0°). (*b*) Velocity field of NGC 1365 obtained from the H92α line observations. The linear gray-scale representation (from 1300 to 1900 km $^{-1}$) indicates the heliocentric velocity.

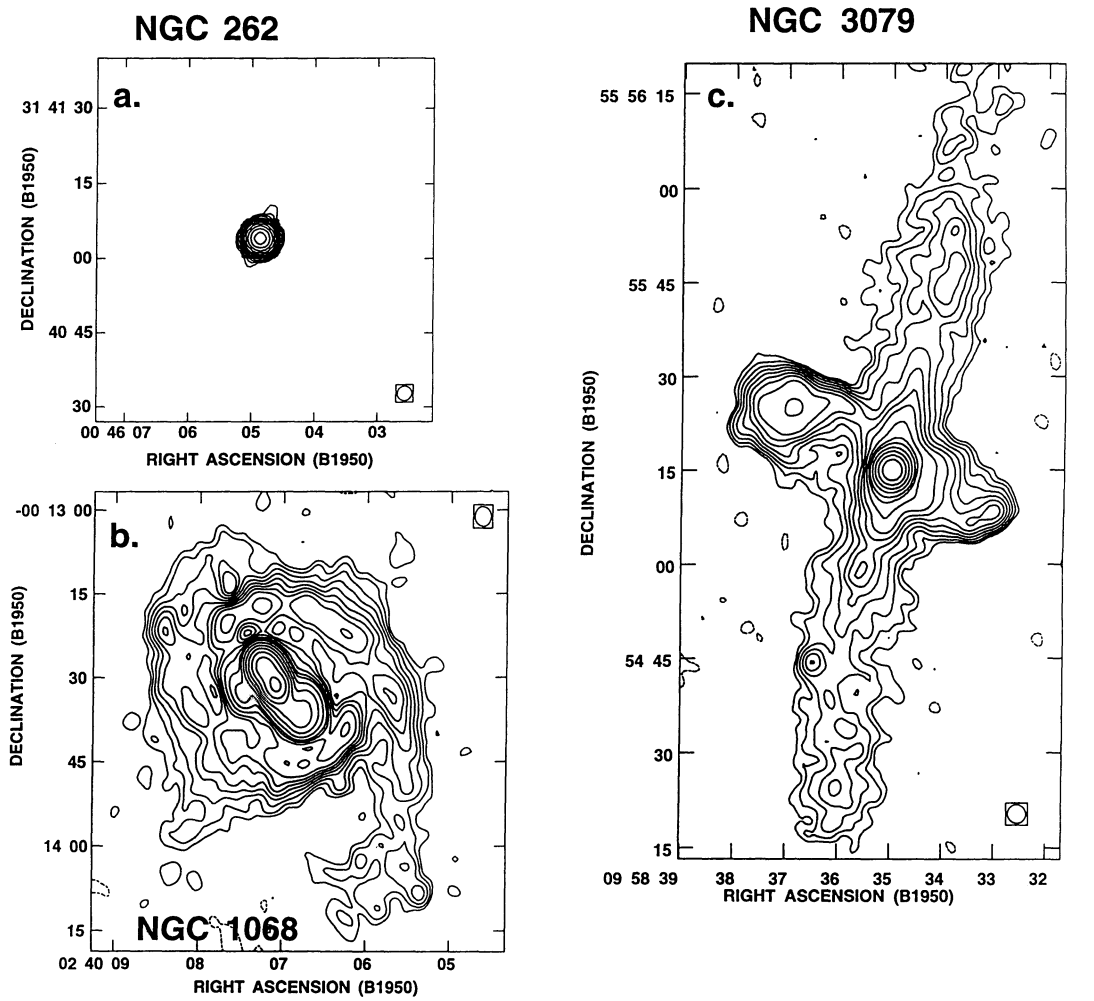

FIG. 5.—Continuum images of three sources where no line is detected. (*a*) Contour plot of the image of NGC 262; the contour levels are −4, 3, 5, 8, 12, 17, 23, 30, 40, 60, 90, 130,... mJy beam^{-1}. The beam size (FWHM) is 2.″9 × 2.″9 (54°), indicated in the lower right corner. (*b*) Contour plot of the image of NGC 1068; the contour levels are −0.16, 0.12, 0.15, 0.32, 0.48, 0.68, 0.92, 1.2, 1.6, 2.4, 3.6, 5.2, 9.6, 19, 38, 77, 154, 307 mJy beam^{-1}. The beam size (FWHM) is 3.″5 × 2.″9 (4°), indicated in the upper right corner. (*c*) Contour plot of the image of NGC 3079; the contour levels are −0.1, 0.075, 0.13, 0.2, 0.3, 0.43, 0.58, 0.75, 1.0, 1.5, 2.3, 3.3, 6, 12, 24, 48, and 96 mJy beam^{-1}. The beam size (FWHM) is 3.″0 × 2.″9 (20°), indicated in the lower right corner.

sities. Although the amplification factor for the line optical depth due to non–LTE effects is large at low densities ($b_n\beta_n \sim -95$ for $n_e = 50$ cm^{-3}, at $n = 92$), the corrected value of τ_L is only ~ -0.003. Since the background continuum flux density is 64 mJy, the contribution from the second term of equation (1) is less than 15% of the observed line strength. The near absence of external stimulated emission implies that similar results will be obtained even if the slab is placed behind the central continuum source.

4.2. *A Collection of* H II *regions*

In this model the observed line is produced by a collection of N H II regions, each of which is characterized by the same temperature (T_e), electron density (n_e), linear diameter (l), and turbulent velocity field (v_t). A similar model has been considered by Puxley et al. (1991) to explain the RRL emission (H53α) observed in the galaxy NGC 2146. This model appears reasonable for a starburst nuclear region, where the H II regions could be created by the young stars born during one or more episodes of starburst and the nonthermal radiation originates in a large number of supernova remnants.

The number of H II regions (N) is determined as follows. The expected peak H92α line intensity, $S_L^{\rm H\,II}$, for a single H II region is computed using equation (1) by replacing Ω_L by $\Omega_{\rm H\,II}$ and multiplying the second term by a factor $1/2\,\Omega_{\rm H\,II}/\Omega_L$. The modification to the second term ensures that only a fraction of the observed continuum is intercepted by a single H II region. The expected width, $\Delta V_{\rm H\,II}$ of the H92α line from a single H II region is calculated using the specified T_e, n_e, and v_t taking into account both thermal and pressure broadening. The number of H II regions (N) is then obtained by dividing the observed integrated H92α flux density (Table 2) by the expected integrated flux density of a single H II region. A combination of T_e, n_e, and l of the H II regions would be considered acceptable if it satisfies all of the following constraints.

1. The number N of H II regions should be confined to the region where the line emission is observed. In other words, the volume filling factor of the H II regions in the nuclear region should not exceed unity. The filling factor is given by $f_{\rm H\,II} = Nl^3/L^3$, where L is the linear size of the line-emitting region.

2. Since the line width due to a single H II region, $\Delta V_{\rm H\,II}$, is much less than the observed line width, $\Delta V_{\rm obs}$, a minimum number of H II regions with different velocities must exist inside every beam area within the line-emitting region. Therefore the number of H II regions (N) must exceed

$$N_{\rm min} = \frac{\langle \Delta V \rangle}{\Delta V_{\rm H\,II}} \times \frac{\Omega_L}{\Omega_B} .$$

3. The peak line intensity of a single H II region ($S_L^{\rm H\,II}$) should not exceed the observed peak line intensity ($S_L^{\rm obs}$).

4. As discussed above, the total thermal emission from the N H II regions should be less than the observed continuum from the nuclear region. In some cases an estimated thermal flux density based on Brγ line emission is available (e.g., Ho, Beck, & Turner 1990). If the continuum optical depth of each of the H II regions is very small ($\tau_C \ll 1$), then the total continuum flux density of N H II regions is given by

$$S_{\rm th} = \frac{2kv^2}{c^2}\,\Omega_{\rm H\,II}\,T_e(1 - e^{-\tau_C}) \times N . \quad (2)$$

As the optical depth becomes large, the effect of shadowing of one H II region by another has to be taken into account. This is done to good approximation by considering the average number of H II regions along any line of sight, which is given by

$$N_{\rm H\,II}^{\rm los} = N \times \frac{l^2}{L^2} . \quad (3)$$

The average continuum optical depth along any line of sight is then $\tau_C^{\rm los} = N_{\rm H\,II}^{\rm los} \times r_C$. The total thermal continuum flux density is given by

$$S_{\rm th} = \frac{2kv^2}{c^2}\,\Omega_L\,T_e(1 - e^{-\tau_C^{\rm los}}) . \quad (4)$$

We have considered a grid of models with T_e, n_e, l in the ranges 1000–12,500 K, 10–10^6 cm^{-3}, and 0.01–100 pc, respectively. The grid values are T_e = 1000, 2500, 5000, 7500, 10,000, 12,500 K; n_e = 10, 50, 100, 500, 1000, 5000, 10,000, 5×10^4, 10^5, 5.10^5, 10^6 cm^{-3}; l = 0.01, 0.05, 0.1, 0.25, 0.5, 1.0, 3.5, 5, 10, 20, 40, 60, 80, 100 pc.

These values cover the entire range from large low-density diffuse H II regions to high-density compact H II regions. Computations made at all possible combinations of the above values (a total of 924) showed that only certain combinations of the parameters satisfied all the constraints. In general, large low-density diffuse H II regions do not satisfy constraint on the total continuum emission. For all the three detected galaxies, models with $T_e > 5000$ K permit only densities above 5000 cm^{-3}. Lower densities are acceptable only if the temperature of the ionized regions is less than 5000 K. For the sources NGC 1365 and NGC 3628 and combination of T_e and n_e are remarkably well constrained for temperatures above 5000 K; only densities in the range 5×10^3 cm^{-3}–5×10^4 cm^{-3} are permitted by the constraints. At T_e = 7500 K, only one value of density (i.e., $n_e = 5 \times 10^4$ cm^{-3}) satisfies all the constraints for the source NGC 1365. Similarly at T_e = 10,000 K, only one value of density (5×10^4 cm^{-3}) passes all the constraints for NGC 3628. For these two sources lower densities are ruled out (if $T_e > 5000$ K) because they produce too much thermal continuum, and the higher densities are excluded because they do not satisfy the line width or peak line intensity criteria discussed above. On the other hand, the densities are not so well constrained for lower temperatures (i.e., $T_e \leq 2500$ K). But then, all these low-temperature models may in fact be highly improbable, unless the abundance of the heavy elements (whose forbidden line radiation can effectively cool the H II regions) is unusually high in the central region of the galaxy.

In the case of IC 694 the models are not so well constrained. This may be because the line region in IC 694 is barely resolved with the present observations and the signal-to-noise ratio is the lowest for the source. Even so, if the temperature of the ionized gas is $\geq$7500 K, then the constraints discussed above rule out densities less than 5000 cm^{-3}. As shown below additional constraints from higher frequency continuum measurements further narrows down the models for IC 694.

The model calculations showed that H II regions with sizes larger than $\sim$10 pc are not permitted by the constraints unless the temperature of the H II regions is less than 2500 K. In fact, for many of the (n_e, T_e) combinations, only a limited range of linear sizes satisfied the constraints. For example, at $T_e = 10^4$ K, $n_e = 5 \times 10^4$ cm^{-3}, only, $l = 0.25 \sim 1.0$ pc pass all the constraints in NGC 3628. Sizes smaller than 0.25 pc produce too much thermal continuum emission and sizes larger than 1.0 pc require too few H II regions and each of such H II regions

produce a peak line intensity which is much higher than that observed in the integrated profile.

In most of these models, the second term of equation (1) (which represents the stimulated emission due to the nonthermal radiation in the nuclear region of the galaxy) makes essentially no contribution to the line emission. This means that the line-to-continuum ratio is not a physically meaningful quantity as the line emission comes from the H II regions and the continuum is mostly nonthermal and there is no external stimulated emission.

For each of the three detected sources (NGC 3628, IC 694, and NGC 1365), the parameters of a typical model that satisfies all the above constraints are presented in Table 5. It can be seen from Table 5 that the model H II regions are optically thick even at 5 GHz. The large opacity of the H II regions is forced by the constraint that the total thermal emission from the N H II regions must be a small fraction of the observed continuum flux density. The recombination line emission from such H II regions must arise in a thin outer layer through stimulated emission. The continuum radiation generated in the interior of the H II region serves as the input to the weak maser near the surface. In such a situation, if the size of the H II region is increased (keeping the density the same), then the line strength increases in proportion to the surface area (i.e. l^2) unlike in the optically thin case, where the line strength increases in proportion to the volume. Although the individual H II regions are optically thick, the volume-filling factor of the N H II regions in the central region is so small (typically $<10^{-5}$) that they will have no appreciable effect on the nonthermal radiation generated in the central region. The effective thermal optical depth along any line of sight is typically less than 10^{-2} (eq. [3]).

The thermal continuum flux density at 5 GHz from the N H II regions computed using equations (2)–(4) are also listed in Table 5. The thermal emission is less than the observed continuum (Table 2) as required by the 4th constraint. The observed continuum consists of both thermal and nonthermal emission and therefore the observed nonthermal flux density can be written as

$$S_{\rm nth} = S_{\rm obs} - S_{\rm th} \ . \qquad (5)$$

The observed nonthermal emission at any frequency is due to some intrinsic nonthermal emission of intensity $S_{\rm nth0}$ modified by the effects of continuum optical depth of the H II regions. The nonthermal emission arises in a region of size L within which the N H II regions are also located, albeit with a small filling factor ($f_{\rm H\,II}$) (Table 5). The H II regions which are located at the far edge of this region will not affect the nonthermal emission. On the other hand, an H II region placed at the near edge of this region will reduce the nonthermal emission by a factor of $e^{-\tau_C}$ where τ_C is the continuum optical depth of the H II region. Since the N H II regions are expected to be distributed randomly in the central region, it is reasonable to assume that on average, every H II region is located half-way inside line-emitting region of size L. Using the number of H II regions along any line of sight given by equation (3), we can then approximate the net observed nonthermal flux density by

$$S_{\rm nth} = S_{\rm nth0}[1 - \tfrac{1}{2}N^{\rm los}_{\rm H\,II}(1 - e^{-\tau_C})] \ . \qquad (6)$$

The above equation works well for all values of $N^{\rm los}_{\rm H\,II}$ if $\tau_C \ll 1$ and for all values of τ_C if $N^{\rm los}_{\rm H\,II} < 1$. Assuming that the intrinsic nonthermal radiation has power-law spectrum (i.e., $S_{\rm nth0} \propto \nu^{\alpha}$) and using measurements of $S_{\rm obs}$ at two frequencies we can solve for both $S_{\rm nth0}$ and α with the aid of equations (2)–(6). The values of $S_{\rm nth0}$ and α, obtained using measurements of $S_{\rm obs}$ from Table 2, are also listed in Table 5.

For the models in Table 5 the expected variation of line and continuum flux density with frequency from the central region of the three galaxies is presented in Figures 6*a* and 6*b*. Line strengths were computed using equation (1) and the total continuum using equations (2)–(6). Available continuum measurements for the three galaxies are also plotted in Figure 6*b*. These models predicted that the line flux density decreases steeply with frequency and that the continuum spectrum will be noticeably modified at higher frequencies due to the pressure of H II regions. It should be noted that these are not unique models. Other combinations of n_e and T_e (which also satisfy the constraints discussed above) will predict slightly different variation of line and continuum strengths with frequency. For example, a model with $T_e = 5000$ K for NGC 3628 will not give as steep and increase in the continuum flux density above 10

TABLE 5

MODEL PARAMETERS OF A COLLECTION OF H II REGIONS FOR THE THREE DETECTED GALAXIES

Parameter (1)	NGC 3628 (2)	IC 694 (3)	NGC 1365 (4)
Electron temperature (K)	10^4	10^4	10^4
Electron density (cm^{-3})	5.10^4	5.10^3	10^4
Number of H II regions	280	110	210
Size (pc)	1.0	5.0	2.5
Filling factor ($f_{\rm H\,II}$)	1.7×10^{-6}	1.6×10^{-5}	9.1×10^{-7}
$N^{\rm los}_{\rm H\,II}$	9.2×10^{-4}	3.1×10^{-3}	5.6×10^{-4}
$\tau_C^{\rm H\,II}$ (at 5 GHz)	28	1.4	2.8
$\tau_L^{\rm H\,II}$ (at 5 GHz)	−1.9	−0.68	−0.83
$S_{\rm th}^{5\ \rm GHz}$ (mJy)	13	7.5	15
$S_{\rm nthO}^{5\ \rm GHz}$ (mJy)	53	100	38
Spectral index ($\alpha_{\rm nth}$)	−1.0	−0.49	−0.82
Total ionized mass ($10^5\ M_\odot$)	1.8	8.8	4.2
$N_{\rm Lyc}$ ($10^{54}\ s^{-1}$)	2.8	1.4	1.3
Fraction of thermal			
Continuum at 5 GHz	17%	7%	29%

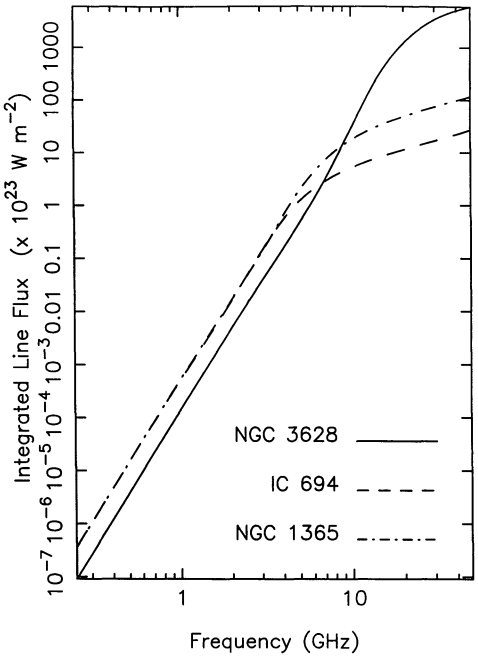

FIG. 6a

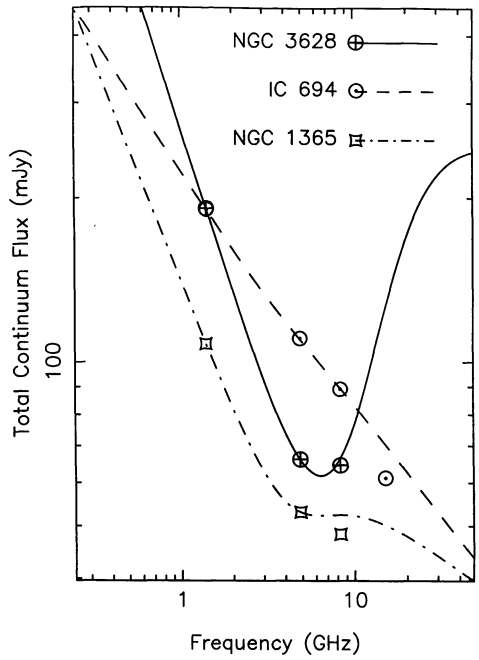

FIG. 6b

FIG. 6.—Expected (*a*) line and (*b*) continuum flux as a function of frequency for the sources NGC 3628 (*solid line*), IC 694 (*dashed line*), and NGC 1365 (*dash-dot line*) computed using parameters of the model in Table 5. The measured continuum flux densities (see Table 2) are also plotted in (*b*) with symbols ⊕ for NGC 3628, ⊙ for IC 694, and ◇ for NGC 1365. The plotted values near 1.4 GHz overlap for the sources NGC 3628 and IC 694.

GHz as indicated in Figure 6*b*. Clearly, higher frequency continuum and line measurements are crucial in determining the validity of the models considered here.

In the case of IC 694, the available continuum measurements provide additional constraints on these models. The measured values at four frequencies (1.4, 4.9, 8.3, and 15 GHz) are plotted in Figure 6*b*. The measured values at four frequencies (1.4, 4.9, 8.3, and 15 GHz) are plotted in Figure 6*b*. The measured continuum flux density at 15 GHz (Carral et al. 1990) require that the maximum allowed electron density is $\sim 5 \times 10^3$ cm^{-3} for any temperature in the range 2500–10^4 K.

5. DISCUSSION

With three new detections, the present observations have doubled the number of galaxies from which RRLs are detected to date all but one of these six galaxies (NGC 253, M82, NGC 2146, NGC 3628, IC 1365) have starburst nuclei. The nucleus of NGC 1365 appears to have Seyfert type II characteristics with normal H II regions surrounding it (Edmunds & Pagel 1982). Although the line was not detected in the Seyfert II galaxies NGC 262 and NGC 1068, the nondetection may be due to the limited velocity coverage of these observations. In Seyfert II nuclei with line widths comparable to those of starburst nuclei, RRLs must be detectable unless the physical conditions (like temperature, and the amount of ionized gas) are quite different from that of starburst nuclei. It would be useful to make similar RRL observations of some Seyfert II nuclei which have relatively narrow Hα line widths ($\sim$300 km s^{-1}). The present observations indicate that the key to detecting RRLs from distant external galaxies is the high sensitivity (noise level $\sim$0.1 mJy beam^{-1}). Figure 6*b* suggests that frequencies above 10 GHz are favorable to detect RRLs.

Another criteria that was used here in selecting the galaxies is the presence of a bright radio continuum core with the assumption that stimulated emission may be important. However, as discusssed in § 4.2 there is hardly any contribution to the line intensity from external stimulated emission (2nd term of eq. [i]). The near absence of external stimulated emission in the model discussed in § 4.2 arises because the volume filling factor of the H II regions is small (see Table 5); the ionized gas intercepts only a small fraction of the nonthermal emission from the central region. It therefore appears that a bright radio continuum core in the central region of the galaxy is not necessarily a good criterion for detectability of recombination lines. In the absence of external stimulated emission, the detectability of RRLs will depend only on the amount of ionized gas present in the nuclear region, the total velocity spread, and the distance to the galaxy. These observations show that some starburst nuclei (and perhaps some Seyfert 2's) satisfy these criteria at distances as large as 41 Mpc (IC 694).

The model discussed in the previous section shows that the intensity of RRLs combined with continuum observations at a few frequencies could provide useful information about the physical conditions, the amount of ionized gas, and the number of Lyman continuum photons in the nuclei of galaxies. Table 5 shows that several hundred H II regions of a few parsecs in size with a total mass of a few times 10^5 $M_\odot$ are required to account for the observed recombination lines. The rate of production of Lyman continuum photons required to maintain the ionization ($N_{\rm Lyc}$) is a few times 10^{54} s^{-1}. If these photons are produced by stars then $\sim$3–7 $\times$ 10^4 O5 stars must be present in the nuclear region of these galaxies. The thermal continuum emission from the H II regions contribute about 5%–30% of the observed continuum at 5 GHz. Since radio recombination lines are unaffected by dust absorption, their measurements can lead to a better estimates of the intrinsic Hα luminosity ($L_{\rm H\alpha}$) which is an important parameter in modeling starburst phenomena (e.g., Gehrz et al. 1983). For example, in

the case of IC 694, from the H92α observations, the inferred Lyman continuum flux is $N_{\rm Lyc} = 1.4 \times 10^{54}$ s^{-1} assuming $T_e = 10^4$ K and $n_e = 5000$ cm^{-3}. The Lyman continuum flux implies an expected Hα luminosity $L_{\rm H\alpha} = 1.9 \times 10^{42}$ ergs s^{-1} ($\sim 4.9 \times 10^8\ L_\odot$) using $L_{\rm H\alpha}$ (ergs s^{-1}) $= 1.37 \times 10^{-12}\ N_{\rm Lyc}$ (s^{-1}) under case B conditions (Osterbrock 1989). The derived Hα luminosity can be compared with the reddening corrected Hα luminosity of 1.9×10^{41} ergs s^{-1} obtained by Armus, Heckman, & Miley (1989), which implies that the extinction may have been underestimated by an order of magnitude.

In addition, the high angular resolution of radio observations and the absence of extinction could make RRLs a very useful tool in studying the kinematics of ionized gas in the nuclear region of starburst and Seyfert II galaxies. As can be seen in Figures 3*b* and 3*c*, the velocity field in the nuclear region of NGC 3628 indicates unusual motions of the ionized gas in the nuclear region. The nuclear rotating disk centered at 900 s^{-1} is obvious in the position-velocity diagram (Fig. 3*c*). This diagram shows that the rotating disk has a diameter of $\sim 5''$ or 270 pc for a distance of 11 Mpc, covering a large velocity range of 280 km s^{-1} (full width at 25% of the peak intensity). Assuming that the ionized gas in the nuclear disk is in circular motion with a maximum rotational velocity of 140 km s^{-1} and a radius of 135 pc, the dynamical mass in the central region is roughly

$$M_D = 2.3 \times 10^5\ M_\odot \left(\frac{V}{\rm km\ s^{-1}}\right)^2 \left(\frac{R}{\rm kpc}\right) \approx 6 \times 10^8\ M_\odot\ . \quad (7)$$

Thus, the fraction of the ionized hydrogen mass in the nucleus to the dynamical mass is $M_{\rm H\,II}/M_D \approx 0.02\%$.

Furthermore, both the anomalous component near 750 km s^{-1} to the west of the nucleus and the extended component near 900 km s^{-1} to the east (Fig. 3*c*) likely have a common origin as suggested from the large-scale H I emission structures (such as the "plume" and "bridge") observed in the surroundings of NGC 3628 (Rots 1978; and Haynes, Giovanelli, & Roberts 1979). The three-dimensional model of the encounter of NGC 3627 around NGC 3628 presented by Rots (1978) indicated that the gas in NGC 3628 is substantially disturbed by the interaction. The velocity field in the central region of NGC 3628 obtained from the H92α observations is consistent with the numerical predictions. The H92α line appears to be a good tracer of the perturbed gas close to the nucleus. The enhancement of the H92α emission line at those specific positions and velocities may also be evidence for the local increase in the formation of early-type stars caused by the galaxy-galaxy interaction.

We thank D. Bhattacharya, Peter Roelfsema, & Peter Shaver for useful discussions and Phil Diamond for help with the software. We also thank J. H. van Gorkom for her many useful discussions and help. The VLA is a part of the National Radio Astronomy Observatory which is operated by the Associated Universities, Inc., under cooperative agreement with the National Science Foundation.

REFERENCES

Anantharamaiah, K. R., & Goss, W. M. 1989, in IAU Colloq. 125, Radio Recombination lines: 25 Years of Investigations, ed. M. A. Gordon & R. L. Sorochenko, 267
Armus. L. Heckman, T. M., & Miley, G. K. 1989, ApJ, 347, 727
Baan, W. A., & Goss, W. M. 1992, ApJ, 385, 188
Bell, M. B., & Seaquist, E. R. 1978, ApJ, , 223, 378
Bell, M. B., Seaquist, E. R., Mebold, U., Reif, K., & Shaver, P. A. 1984, A&A, 130, 1
Boisse, P., Cassoli, F., & Combes, F. 1987, A&A, 173, 229
Carral, P., Turner, J. L., & Ho, P. T. P. 1990, ApJ, 362, 434
Churchwell, E., & Shaver, P. A. 1979, A&A, 77, 316
Condon, J. J., Condon, M. A., Gisler, G., & Puschell, G. 1982, ApJ, 252, 102
Condon, J. J., Huang, Z.-P., Yin, Q. F., & Thaun, T. X. 1991, ApJ, 378, 65
Cornwell, T. J., Uson, J. M., & Haddad, N. 1992, A&A, 258, 583
Edmunds, M. G., & Pagel, B. E. J. 1982, MNRAS, 198, 1089
Fabiano, G., Heckman, T. M., & Keel, W. C. 1990, ApJ, 355, 442
Gehrz, R. O., Sramek, R. A., & Weedman, D. E. 1983, ApJ, 267, 551
Haynes, M. P., Giovanelli, R., & Roberts, M. S. 1979, ApJ, 229, 83
Ho, P. T. P., Beck, S. C., & Turner, J. L. 1990, ApJ, 349, 57
Israel, F. P., Baas, F., & Maloney, P. R. 1990, A&A, 237, 17
Ondrechen, M. P., & van der Hulst, J. M. 1989, 342, 29
Osterbrock, D. E. 1989, Astrophysics of Gaseous Nebulae and Active Galactic Nuclei (Mill Valey, CA: Univ. Science Books)
Puxley, P. J., Brand, P. W. J. L., Moore, T. J. T., Mountain, C. M., & Nakai, N. 1991, MNRAS, 248, 585
Roelfsema, P. R., & Goss, W. M. 1992, A&A, Rev., 4, 161
Rots, A. H. 1978, AJ, 83, 219
Salem, M., & Brocklehurst, M. 1979, ApJ, 39, 633
Sandqvist, A., Jorsater, S., & Lindblad, P. O. 1982, A&A, 110, 336
Sarazin, C. L., & Wadiak, E. J. 1983, A&A, 123, L1
Sargent, A., & Scoville, N. 1991, ApJ, , 366, L1
Schmelz, J. T., Baan, W. A., & Haschik, A. D. 1987a, ApJ, 315, 492
———. 1987b, ApJ, 320, 145
Seaquist, E. R., & Bell, M. B. 1977, A&A, 60, L1
Shaver, P. A. 1975, Pramana, 5, 1
———. 1978, A&A, 68, 97
Shaver, P. A., Churchwell, P. A., Churchwell, E., & Rots, A. H. 1977, A&A, 55, 435
Teuben, P. J., Sanders, R. H., Atherton, P. D., & van Albada, G. D. 1986, MNRAS, 221, 1
Viner, M. R., Valee, J. P., & Hughes, C. A. 1979, AJ, 84, 1335
Wilson, A. S., & Nath, B. 1990, ApJS, 74, 731
Young, J. S., Xie, S., Kenny, J. D. P., & Rice, W. L. 1989, ApJS, 70, 699